GABOR FILTER AND TEXTURE FEATURES BASED IMPROVED FINGER VEIN AUTHENTICATION

K. SANTHOSH KUMAR[1], D. MAHESWARI[2]

[1]Research Scholar, Rathnavel Subramaniam College of Arts and Science. E-mail: bbksan@gmail.com
[2]Research Coordinator, School of Computer Studies. PG, Rathinavel Subramaniam College of Arts and Science.

ABSTRACT

Recently, biometric recognition has emerged quite popular in various advanced human authentication systems like secure access control systems, forensic applications and criminal identification systems etc. It is a technique to identify a human automatically with the help of a computational algorithm using the biometric features present in database. Finger vein features based recognition is also a type of the biometric authentication systems used in this study. In the earlier work, Corner detection algorithm is utilized for the extraction of features, so called corner points from finger vein image, and pattern matching was carried out according to differences between corners denoted as points employing the neural network classifier. But, if finger-vein images quality are not up-to-the mark, segmentation errors might crop up while the vein patterns are extracted (binarized). In order to resolve this problem, texture feature extraction is performed with the help of grey level co-occurrence matrix in this work. For improving finger-vein images perceptibility during the pre-processing of the feature extraction technique, scattering removal and vein enhancement techniques have been also presented in this study. This research work uses thinning and denoising for the removal of the unnecessary pixels in the vein pattern. Corner detection is carried out with the help of the Harris corner detection operator and the tracking of the finger vein branches will be carried using Improved Fuzzy c-means Clustering   algorithm. At last, Morphological dilation and dot product operations are carried out on extracted finger vein to increase pixel quality and to get the real or fake finger vein image depending on User-defined threshold.

Keywords: Biometric Authentication, Texture Feature Extraction, Vein Enhancement, Genuine, Imposter And   User-Specific Threshold.

INTRODUCTION

Personal identification is one of the important tasks undertaken in security system. Conventionally, password or Personal Identification Numbers (PINs) key etc are utilized in security system. However, these authentication means are forgotten easily. This issue is resolved by biometric pattern application. Biometrics is the technology that is employed for the authentication of human beings exploiting the distinctness of his or her physiological and behavioral aspects. Therefore, it is utilized as an alternate to the classical authentication mechanisms [1, 2, 3].

Generally, biometric patterns such as finger print, iris, face etc are used. However, all these biometric traits can be easily stolen by malicious intruders. In this, non-counterfeit able biometric pattern is taken into consideration. Finger Vein is a remarkable biometric pattern in terms of security as well as simplicity. Finger vein system can be applied only on a live human body, since the infrared camera can click the image only if there is hemoglobin in the body. A finger vein pattern is unmissable and is unique for each person. It is extremely secure as the vein pattern is present inside the body and replicating and reusing it is hard and impossible [4, 5].

Finger vein recognition system can make use of low resolution images. In the earlier work, Corner detection algorithm is utilized for the extraction of features, so called corner points from finger vein image,, and pattern matching was carried out according to the differences between corners denoted as points employing the neural network classifier. But, if finger-vein images quality are not up-to-the mark, segmentation errors might crop up while the vein patterns are extracted (binarized). In order to resolve this problem, texture feature extraction is performed with the help of grey level co-occurrence matrix in this work. For improving finger-vein images perceptibility during the pre-processing of the feature extraction technique, scattering removal and vein enhancement techniques have been also presented in this study [5, 6, 7]. In this research work, thinning and denoising are carried out to eliminate the unnecessary pixels from the vein pattern. Corner detection is carried out with the help of the Harris corner detection operator and the tracking of the finger vein branches will be done with Improved Fuzzy c-means Clustering algorithm. At last, Morphological dilation and dot product operations are carried out on extracted finger vein for increasing the pixel quality and to get the real or fake finger vein image depending on User-defined threshold. [8,9,10].

LITERATURE REVIEW

This section provides a review on the various finger vein authentication systems that uses feature extraction techniques, image enhancement approaches and neural network classifier. Das et al [2018][11]   introduced a finger vein identification system that depends on convolutional-neural-network and discussed network performance on four openly-available databases are analyzed. Primary objective of this research work is for introducing a deep-learning technique to identify finger-vein, which is capable of achieving consistent and appreciably superior performance on working with finger-vein images of diverse qualities. Results of comprehensive bunch of experiments reveal that accuracy attainable with the discussed technique can exceed above 95% right identification rate for each of the four openly-available databases. Tagkalakis et al [2017][12]recommended a novel finger vein authentication technique, which depends on the effective identification of the non-vein areas, with the aim of defining the primary vein patterns. The discussed technique exhibits robustness in the extraction and depiction of not just finger vein pattern, but also few other significant features like width of the veins. The authentication algorithm is assessed using a database with 400 finger vein images. The false acceptance and rejection rates attained are 0% and 0.5% correspondingly.

Yang et al [2019][13]   proposed anew technique known as FV-GAN for finger vein extraction and verification, which depends on generative adversarial network (GAN) regarded to be the primary effort made in this field. Different from other CNN-based techniques, FV-GAN learns from the combined dissemination of finger vein images and pattern maps instead of having a direct mapping between them, holding to the objective of gaining a better resilience against outliers and vessel outages. In addition, FV-GAN uses fully convolutional networks in form of elementary framework, and eliminates fully connected layers, which eases limitation on size of the input image and minimizes computational cost involved in feature extraction process. In addition, an adversarial training mechanism is designed and a hybrid loss function for FVGAN is proposed. The findings achieved on experiments carried out on two openly available databases reveal a considerable enrichment by using FV-GAN in the verification of finger veins with respect to both the metrics of verification accuracy and equal error rate.

Yang et al [2019][14] demonstrated a novel finger identification system for acquisition of dorsal finger vein's unified pattern and texture in one unique image with just one camera. It helps in efficient reduction of the expenditure and size of imaging device used for multi-modal patterns acquisition. The dorsal finger vein and texture's unified pattern saves both memory and computation. The results of experiments show that novel system and feature not just saves disk space and computation, but is more essentially, efficient for identification task. The performance of discussed PWBDC technique is quite good on both newly created database made up of mixed images and a common open database of classical finger vein images, which is far superior compared to several popular and benchmarked techniques.

Shazeeda and Rosdi[2018][15]studied about an effective classification technique for finger vein identification known as mutual SRC (MSRC). This technique categorizes the test sample using an innovative decision rule that considerably increases traditional SRC's recognition rate. Using this proposed decision rule,   test sample is classified not just on basis of closest sparse neighbour but also on deciding training samplesthat uses test samples in the form of its nearest neighbour (NN). As per this technique, it is noticed that an improvement of 4.67, 10.59, 26.82, and 3.44% in recognition rates is achieved for novel MSRC technique in comparison with classical SRC that uses four openly available finger vein database.

Meng et al [2018][16] presented afresh approach for achieving finger vein identification. This technique, which considers the distortion to be distinct information, is different from the available techniques, which try neglecting the impact of distortion. The novel approach depends on the perspective that regular distortion, which is associated with a change in posture, is only observed in real vein patterns. With regard to the technique, optimized matching is incorporated for generating the pixel based 2D movements, which are associated with distortions. The texture of evenness obtained from the displacement fields is considered to be the ultimate matching score. The validation of PolyU and SDU-MLA has been done through comprehensive experiments on two openly available databases and it is shown that the discrimination of the new feature extracted from distortions is much better. The equal error rate (EER) attained is the least in comparison with that of benchmarked approaches.

Prabu   [2017][17] recommended an innovative quality estimation algorithm for the estimation of the vein quality and the vein image is improved with the help of multi scale matched filtering. In the case of vein extraction, the information depicted by the modified image and the vein quality is aggregated employing SVM classifier.

The discussed vein extraction process can deal with the challenges of of hair, skin texture and different veins widths such that the extraction of real veins is accurate. The results of experiments show that the novel system has attained an accuracy of 98.59 % and its performance is quite better compared to other earlier systems and is efficient in achieving security.

PROPOSED   APPROACH

This section studies the finger vein identification process extensively. It has seven units and first one comprises of denoising and thinning, second one is made up of Scattering   removal, and the third   one   includes Vein   enhancement, with the fourth one comprises of the feature   extraction process, fifth one incorporates corner detection , sixth one includes the   bifurcation

detection, with the seventh step being branch tracking, eighth one includes Morphological dilation and dot product, ninth one involves User-defined threshold selection and recognition. Fig. 1. depicts the framework of the discussed work.
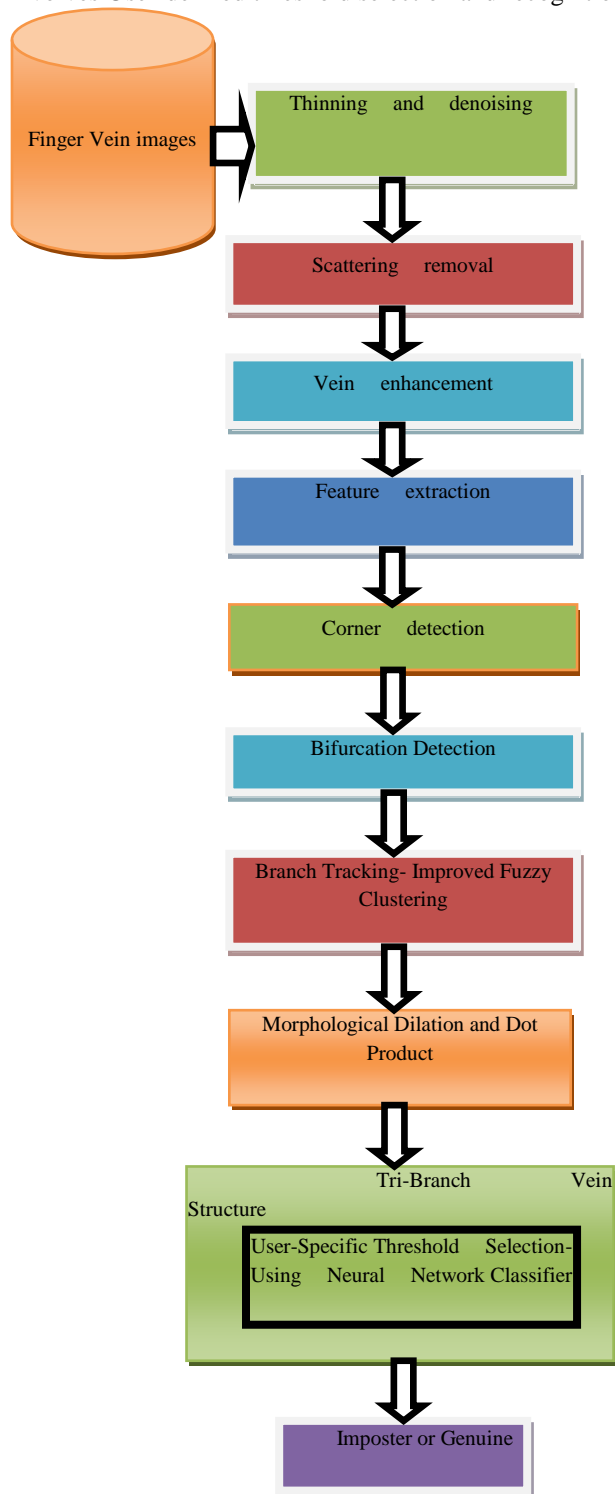
Fig.1: Overall architecture of the proposed methodology

Thinning and Denoising

Fig. 2: Extracted vein image from the database

Fig.2. shows the Extracted vein image from the database Thinning is carried out by finding region's skeleton applying the skeletonization process also known as thinning. Mathematical morphology operators is used for computing this. In this technical work, it is associated with hit or miss transform. The image thinning I using a structuring element $J = (J_1, J_2)$ is expressed by:

$$T\square in(i,j) = i - (i \otimes j) \tag{1}$$

Where, subtraction is really the logical subtraction given as:

$$X\text{-}Y = X \cap NotY \tag{2}$$

The operation is performed again and again until there are no more changes that can be made to image (i. e., till convergence point). Structuring element sequence J is user-defined. Thinning of the image is done with structuring element pairs (J_1^i, J_2^i), $i = 1..8$ in sequence. By this, image's connected skeleton is produced. Morphological thinning operation is employed for acquiring vein network (single-pixel wide) from vein patterns.

In the domain of digital imaging, acquisition techniques and systems introduce various kinds of artifacts and noises. Also, noisy image results in poor visual quality, and also minimizes perceptibility of objects with poorer contrast. In the case of vein network, intersection point of burr and vein branch can be wrongly taken to be bifurcation point. Hence, burr is identified and eliminated based on its length, as the burr is much tinier in comparison with the real vein branch. Then this denoised vein image will become the input to the scattering elimination.Fig.3. shows the thining results.

Fig. 3: Thinning results

Scattering   Removal

The NIR lights that penetrate through a human finger can go through absorption, reflection, scattering, and refraction by such finger parts like skin tissue, blood vessels, muscles and bones. This concept is identical to that of light being scattered in fog, which can lead to extreme reduction in the image scenes' visibility. Therefore, finger–vein image deterioration is unavoidable owing to high scattering behavior of biological tissue. Certainly, image restoration employing scattering suppression helps in improving finger–vein images quality. Fore limitation of scattering effect from the images, dehazing methods are employed in this technical work [18, 19, 20].

Suppose that I(x,y) refers to shot image, R(x,y) indicates realhaze-free image, q(k) represents atmospheric medium's extinction coefficient and d(x,y) stands for scene's depth-map, Koschmieder's law defined below is generally utilized for the restoration of the deteriorated image.

$$I(x,y) = R(x,y)e^{-\rho(\lambda)d(x,y)} + I_s\left(1 - e^{-\rho(\lambda)d(x,y)}\right) \tag{3}$$

Where, λindicates light wavelength and $I_s$stands for environment luminance around. More or less, the Koschmieder's law is used for solving the problem of finger–vein image reconstruction as atmospheric particles and biological tissues form two light dispersing mediums having dissimilar extinction coefficients associated with distinct light wavelengths.

Unfortunately, it is hard for obtaining actual $\rho(\lambda$, I_s and d(x,y) practically, image restoration as per Eq. (3) and therefore this is an ill-presented problem. Rather than getting an improved estimation   for $\rho(\lambda$, I_s and d(x,y) correspondingly, filter technique is used here for estimating medium veil intensity υ (x,y) = I_s(1- e$^{-\rho(\lambda)d(x,y)}$). Presume that I_s is a constant, by solving Eq. (3) based on R(x,y),   the following equation is obtained

$$R(x,y) = I_S\left(1(x,y) - v(x,y)\right)/\left(I_s - v(x,y)\right) \tag{4}$$

This technique can help in the successful implementation of visibility restitution process from   a single image with a speed that is remarkable. As far as the best of knowledge goes, this is regarded to be first try made in improving image dehazing based

finger–vein visibility. It can be observed that scattering removal (SR) can enhance the image visibility obviously and in the next step, this output image will become the input to the image enhancement step.

Finger-Vein Image Enhancement

A set of Gabor filters are introduced for the process of image enhancement. A set of acceptable even symmetric Gabor filters can be defined as

$$G_m^k(x,y) = K \exp\left\{-\frac{1}{2}\left(\frac{x_{\theta_k}^2 + \gamma^2 y_{\theta_k}^2}{\sigma_m^2}\right)\right\}\left(cos\left(2\pi f_m x_{\theta_k}\right) - exp\left(-\frac{v^2}{2}\right)\right) \qquad (5)$$

where $K = \gamma/2\pi\sigma_m^2$, $x_{\theta k} = x\cos(\theta_k) + y\sin(\theta_k)$, $y\theta_k = -x\sin(\theta_k) + y\cos(\theta_k)$, $m(= 1, 2, \cdots, M)$ indicates scale index, $k(= 1, 2, \cdots, N)$ stands for orientation index, θ_k represents an orientation, $\sigma_m f_m$ and γ correspondingly indicate mth scale, center frequency and elliptical Gaussian envelope aspect ratio. Let $\Delta\phi \in [0.5, 2.5)$ refer to frequency bandwidth in unit of octaves, $K_a = (2^{\Delta\phi} + 1)/(2^{\Delta\phi} - 1)$, $\varsigma = (1 + K_a)/(1 - K_a)$ and $v = \sqrt{2}\ln 2/Ka$, to maintain a non-overlapped spacing between two neighboring scales in frequency domain, as shown in Fig. 2(b), the following relationship has to be maintained,

$$f_m = f_{m-1}\varsigma^m, \quad \sigma_m = \frac{\sqrt{\ln 2/2}}{f_m k_\alpha \pi} \qquad (6)$$

Let $\hat{I}_0(x, y)$ refer to an restored image $I_0(x, y)$'s negative version and $U_m^k(x, y)$ stand for a Gabor transformed image, and the following expression is got

$$U_m^k(x,y) = G_m^k(x,y) \otimes \hat{I}_0(x,y) \qquad (7)$$

Where, symbol $\otimes$" represents 2D convolution. For a certain scale, value of $U_m^k(x, y)$ has to be maximum when an adaptable Gabor filter has a concurrent and local match with vein ridge's width and orientation [21,22]. Therefore, to eliminate this unnecessary information efficiently, a multiscale multiplication rule (MSMR) is proposed, which is expressed as

$$E(x,y) = \prod_{m=1}^{M} \theta_{k \in (0,\pi)}^{\max\left(U_m^k(x,y)\right)} \qquad (8)$$

Therefore, even Gabor filters optimal responses in M scales and N orientations is concurrently attained with MSMR usage. This is extremely desirable while enhancing the vein vessels having orientation and diameter differences. These enhanced images will be provided as an input to feature extraction step.
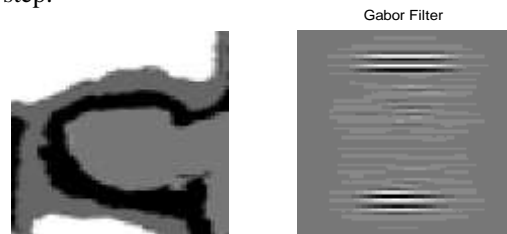
Fig. 4: scattering removal and vein enhancement results

Texture Feature Extraction Employing Grey-Level Co-occurrence Matrix

The Grey-Level Co-occurrence Matrix (GLCM)) is efficient in estimation of the image features correlated with second-order statistics. In fact, a GLCM refers to a matrix in which the number of rows and columns are equal to the number of gray levels, G, existing in image. Matrix element P (i, j | Δx, Δy) gives the relative frequency with which two pixels, having a pixel distance (Δx, Δy) between them, are found within a particular adjacent region, one having an intensity 'i' and the other having an intensity 'j'.

At a certain displacement distance d and °, 90°, 45°at a specific angle (ө), for differences between gray levels 'i' and 'j', second order statistical probability values are depicted using matrix element P (i, j | d, ө). A displacement, d could use a value of 1, 2, 3… n while an angle, ө is restricted to 0°and 135),° and 135°, 90°, 45°[25].

From the experiments, it can be seen that the GLDM feature descriptor computation is done from five angle values ө (0 five texture features (Entropy, Homogeneity, correlation, contrast, Energy) and displacement distance d=1 hence, realization includes twenty features. The texture features are computed as follows: Energy: Energy defines evenness found in mammographic image. Usually, energy is computed from mean squared signal value. Its formula is given as below

$$\text{Energy} = \sum_{i,j=0}^{n-1} p(i,j)2 \qquad (9)$$

Contrast: The contrast measures difference between least and greatest values of pixels group existing in neighbourhood[23]. It computes the amount of t local variations existing in the image

$$\text{Contrast} = \sum_{i,j=0}^{n-1}(i-j)^2 p(i,j) \qquad (10)$$

Correlation: It renders correlation value of a pixel with its neighbour over whole image.

$$\text{Correlation} = \sum_{i,j=0}^{n-I} \frac{(i \times j)p(i,j) - u_i u_j}{\sigma_i \sigma_j} \qquad (11)$$

$\sigma 2$ = intensities variation of each and every reference pixels in relationships, which have contributed to GLCM, formulated as below:

$$\theta^2 = \sum_{i,j=0}^{N-1} p_{i,j}(i\text{-}u)\,2 \qquad (12)$$

Homogeneity, Angular Second Moment (ASM): ASM used for the homogeneity measurement of the image

$$\text{Homogeneity} = \sum_{i=0}^{n-1} \sum_{j=0}^{n-1} \{p(i,j)\}^2 \qquad (13)$$

Entropy: It defines the measure of non-uniformity or complexity observed in image. Entropy attains the biggest value if P (i, j) values are allocated very uniformly throughout whole matrix. Entropy exhibits a high but an inverse correlation with Energy.

$$\text{Entropy} = -\sum_{i,j=0}^{n-1} p(i,j)\log p(i,j) \qquad (14)$$

Where, 'i' refers to the rows of the GLCM matrix, 'j' indicates the columns of the GLCM matrix, 'n' refers to the number of gray levels and P(i, j) indicates the cell that the row and the column of the GLCM matrix represents.

Based on these evaluations, the extractions of the texture features are achieved. After this, it will be taken to be the input for corner detection process [24, 25].

Corner Detection Employing Harris Corner Detection Algorithm

At present, there are two divisions in comer detection: image edge extraction algorithm is used in one division and image grey comer detection is used in second division [21].

A class of extraction operator is Harris comer detection algorithm and signal point feature forms base for this. Image's first derivative are used in this. In any direction, image window (j) and its intensity variation is defined as,

$$E_{x,y} = \sum w_{x,v}\left[I_{x+v,y+v} - I_{w,v}\right]^2 = \sum_{w,v} xX + [yY + O(x^2,y^2)]^2 \qquad (15)$$
$$= Ax^2 + 2Cxy + By^2 \qquad (16)$$
$$= (x,y)M(x,y)^r \qquad (17)$$

Where, M $= \begin{bmatrix} A & c \\ c & B \end{bmatrix}$, among them A=X2 $\otimes$ w,   B=y2$\otimes$ w, C = (XY) $\otimes$ w , X and Y refers to first-order gray gradient, they are derived by finding the image convolution,

$$X = \frac{\partial I}{\partial x} = I \otimes (-1,0,1)\quad Y = \frac{\partial I}{\partial V} = I \otimes (-1,0,1) \qquad (18)$$

With the aim of improving noise resilience, Gaussian approach is used for smoothening the image window, and the Gaussian window is devised as per the formula given

$$w_{w,v} = \exp\left[-\frac{1}{2}(u^2 + v^2)/\delta^2\right] \qquad (19)$$

Two eigenvalues of Mare defined as λ_1 and λ_2 and M's rotation invariants are referred as λ_1 and λ_2, and it is proportional to local autocorrelation function's principal curvatures. At this junction, λ_1 and λ_1's value feature are used for computing edges, corners and flat regions and there are three conditions:

(1) If two small curvatures, flat region can be depicted;

(2) With one small and one large curvatures, partial autocorrelation function is same as ridge as indicated, and change along ridge is small, whereas change opposite to ridge is large, it depicts an edge.

(3) Peak value is indicated with two big curvatures and strong variation along any direction is shown and it indicates a corner point.

Using matrix M, Comer Response Function (CRF) is represented as,

$$CRF = \det(M) - k.t^2(M) \qquad (20)$$

Where, determinant of M is represented as det(M}, M's matrix trace is represented as t, in general constant k is fixed as point with local maximum CRF is comer.

Complete flow is given as below,

Step I: For every pixel (x,y) in gray image I, the correlation matrix M is calculated;

Step 2: Comer score of respective pixels are approximately computed;

Step 3: To reduce extracted corner count, fixed the CRF threshold.
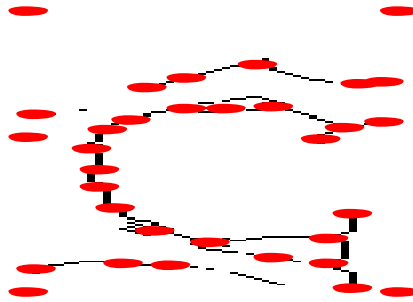
Fig. 5: Results of corner detection

Fig. 5. depicts the results of corner detection. Using the above technique, the extracted edges will be utilized for bifurcation detection**.**

3.6. Bifurcation   Detection

In general, one bifurcation point is connected with three vein branches. In can be stated that, there are six switching number between 0 to 1 in eight adjacent bifurcation points. According to this, designed the bifurcation detection technique. Current point is represented as p(x; y) and its eight neighbourhood points are represented as $\{P_i = p_1, p_2....p_8\}$. Point p(x; y) is regarded as a bifurcation, if t value of N_s are equivalent to six, defined as follows: Fig.6. results of bifurcation points detection.

$$N_s = \sum_{i=1}^{8}|p_i + 1 - p_i|, \hspace{4cm} (21)$$

Where $p_9 = p_1$
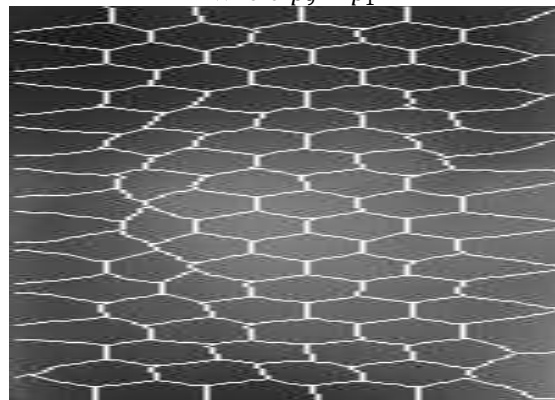
Fig. 6: Results of Bifurcation points detection

After this, this bifurcation points identified will become the input for branch tracking in the next step after improved fuzzy c means algorithm application**.**

Branch Tracking Employing Improved Fuzzy c-Means   Clustering   Algorithm

A class of unsupervised clustering algorithm is Fuzzy c-mean clustering, which is utilized most popularly in computer vision and image processing because of its easy deployment and its performance in clustering.

The FCM algorithm's   important disadvantages include:

(1) It shows sensitivity to point in isolation.

(2) Prior requirement of fuzzy weighted index m and number of clustering c and clustering outcomes are directly affected by   c and M values.

(3) It falls into local extreme point or saddle point rapidly and cannot attain optimal answer.

To get over those problems, this work is involved with the improvement of the fundamental fuzzy c means algorithm.

1.   A modified Fuzzy C-Means Clustering Algorithm

Here, introduced a modified fuzzy C-means clustering algorithm. Incorporation of a weighted value with membership degree of data object is a basic principle and clustering number c are optimized by adding fuzzy clustering validity function with this algorithm. Following describes the IFCM algorithm,

Initialization: Clustering number is initialized as c, $2 \leq c \leq n$, where, amount of image pixel are represented as n, the original clustering pattern $P^{(0)}$, iterative counter $b=0$, deciding the iterative threshold ε.

Step 1 Partition matrix $U^{(b)}$ is updated or computed

Step 2 Clustering pattern matrix $P^{(b+1)}$ is updated for i1… c

Step 3 If $p^{(b)} - p^{(b+1)} < \varepsilon$, then terminates the algorithm and export the pclustering pattern P   and partition matrix U, else let b=b+1, go to Step 1.

Step 4 .Value of $FP^{(b+1)}$ (U; c) ,   if $FP^{(b+1)}$ (U; c) <$FP^{(b)}$ (U; c) computed, then c = c +1, go to step 1, else, validity function FP (U; c) value gets minimum, and clustering number c = c-1, complete the clustering process.

Using the steps, the identification of single-pixel wide tri branch vein structure (i.e., bifurcation and its local branches) is done and it is illustrated in fig.7 below. Then it will be enhanced using few morphological operations in the step that follows

Fig. 7: Results of Clustering

Morphological   Dilation and Dot Product

A fresh binary image is produced by performing morphological operation on a binary image, where, a non-zero pixel is produced by this operation at the position of input image having successful test. In this technical work, on single-pixel wide tri-branch vein structure, performed the morphological dilation operation, where   8×8 matrix is used as a structuring element with an elemental

value of 1. For matching process, tri-branch vein map is obtained by performing dot product between whole vein pattern and dilated form. After this, this newly identified visibility enhanced vein image becomes the input to the last step of authentication.

Correlation Filter Based User-specific Threshold Selection Employing Neural Network

Similarity between finger vein images of the individuals is computed with the help of User-specific Threshold Selection based on neural network for real images and fake images classification.

Layer 1:

Fuzzification layer forms the first layer. Each node i in this layer is depicted as a square node and defined by:

$$O_i^1 = \mu \ _{A_i}(x) \ for \ i = 1,2 \tag{22}$$

$$O_i^1 = \mu \ _{B_{i-2}}(y) \ for \ i = 3,4 \tag{23}$$

Where, x and y stands for the node *I's input* and outputs are computed by input's fuzzy membership grade. For calculating membership degree of the input, every node makes use of Gaussian membership function.

$$o_i^1 = \mu_{Ai}(x) = e^{\frac{-1}{2}\left(\frac{x-c_i}{\sigma_i}\right)} \tag{24}$$

Where $\{c,\sigma\}$ specifies a parameter set. Membership function's center is represented as C and σ determines the width of the membership function. These parameters are known as premise parameters.

Layer 2:

The second layer is a Rule layer. In this layer, membership functions form input values and every node carries out the multiplication of the inputs and yields the output representing the firing strength of rule. This layer's output is expressed in equation as

$$O_i^2 = w_i = \mu \ _{A_i}(x)\mu_{B_i}(y), \ i = 1,2 \tag{25}$$

Layer 3:

Here, i-th node is found by ratio of i-th rules firing strength to summation of firing strengths of all rules.

$$O_i^3 = w_i = \frac{w_1}{w_1+w_2}, \ i = 1,2 \tag{26}$$

Layer 4:

In this layer, adaptive nodes are formed by nodes.

$$O_i^4 = w_i f_i = w_i(p_i x + q_i y + r_i) \tag{27}$$

Where, (w) refers to layer 3 output, and $\{p_i, q_i\}$ indicates parameter set also known as consequent parameters.

Layer 5:

This layer comprises of single static node. Here, overall output is computed as the sum of every incoming signal, expressed in equation below

$$O_i^5 = \sum_{i=1} w_i f_i = \frac{\sum_i w_i f_i}{\sum_i w_i} \tag{28}$$

In accordance with the layer function, the similarity between the two input finger vein images is computed for all users and then this similarity score will be saved and utilized for matching with the registered user to prevent the fake images. Fig. 8. shows the ANFIS architecture.
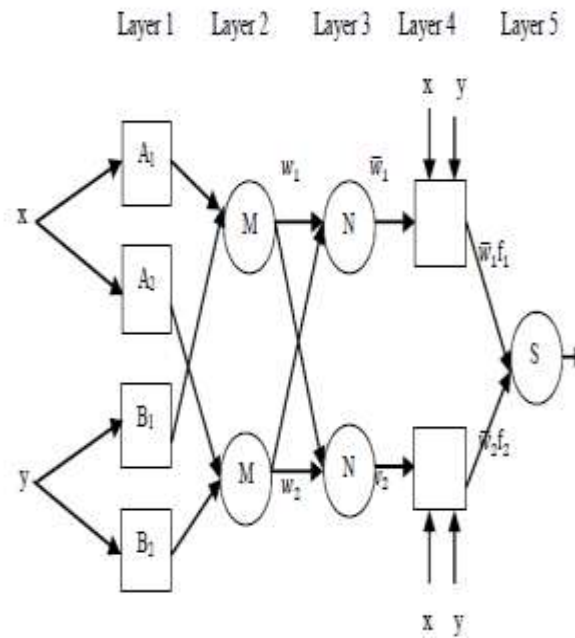
Fig.8: ANFIS Architecture

RESULT AND DISCUSSION

This sections presents experimentation results carried out on proposed approaches. The proposed approach is implemented in MATLAB2012 on a PC having a CPU 3.60GHz, 12.00G memory and in the next step, the comparison analysis is carried out using availableuser specific threshold based filtering (USCBF) ,   Aanatomy Structure Analysis-based vein extraction (ASAVE), and new correlation filter based selection with genetic algorithm (CFBGN) with discussed User Specific Threshold Selection employing ANFIS (USTS-ANFIS) in terms of the metrics of error rate, accuracy, precision, recall and false rejection rate for Hong Kong Polytechnic University (HKPU) database finger vein images. In this database, there are 12 images in every one of first 210 fingers, clicked in two session, and there are6 images in every one of final 103 finger, clicked in one single session. Images are 8-bit gray level BMP file with a resolution of 513_256 pixels . Table 1 shows the results of the performance comparison analysis

Table 1: Performance   comparison   results

Techniques	Metrics				
	Precision	Sensitivity	Accuracy	Error Rate	F-measure
ASAVE	81.1900	83.4000	83.2500	16.7500	82.2900
USCBF	88.9100	88.9700	89.0200	10.9800	88.9400
CFBGN	91.8300	92.0033	91.8600	8.1400	92.0033
USTS-ANFIS	92.5300	93.0053	92.7788	7.2212	93.0044
GLCM -ANFIS	95.4840	95.5836	95.5285	4.4715	95.5338
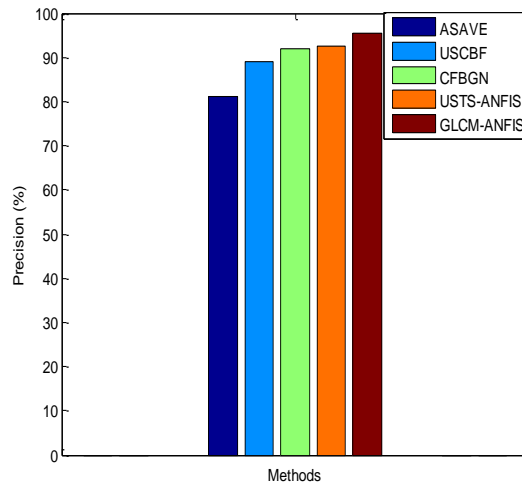
Fig. 9: Precision results of various techniques

Fig. 9. Shows the precision metric results of various techniques. The results of performance comparison between GLCM-ANFIS and the existing ASAVE, USCBF, CFBGN and USTS-ANFIS techniques are illustrated in the figure above in terms of precision. Dehazing of scattering removal helps in the image quality improvement such that it automatically boosts the precision results of finger vein authentication process. It is confirmed from results that discussed GLCM-ANFIS model yields much better precision results of 95.4840% whereas existing ASAVE, USCBF, CFBGN and USTS-ANFIS attains only 81.1900%, 88.9100% , 91.8300% and 92.5300% respectively.
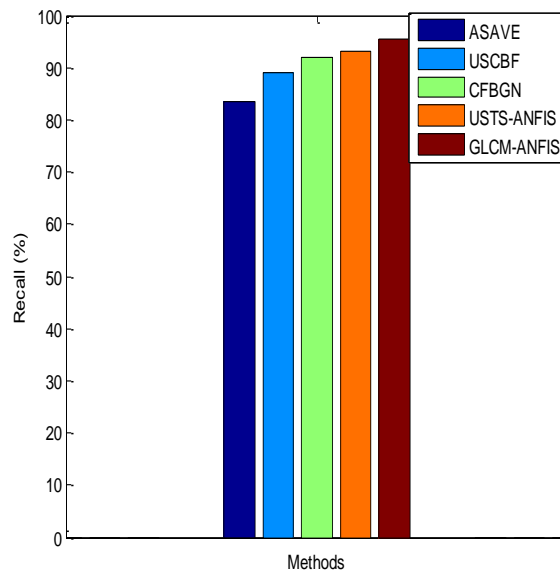
Fig. 10: Recall   results   of   various techniques

Fig.10. shows the recall   results   of   various techniques. Efficiency of discussed GLCM-ANFIS technique is proven through its comparison with existing ASAVE, USCBF, CFBGN and USTS-ANFIS with respect to **Recall** metric. It is confirmed from results that discussed GLCM -ANFIS yields much better **Recall** results of 95.5836% whereas existing ASAVE, USCBF, CFBGN and USTS-ANFIS attains only83.4000%, 88.9700% , 92.0033% and 93.0053%respectively.
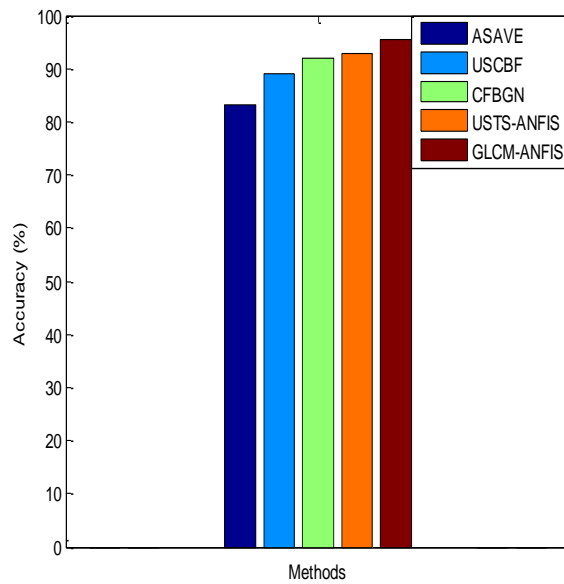
Fig. 11: Accuracy results of various techniques

Fig.11. shows performance comparison result of GLCM-ANFIS and existing ASAVE, USCBF, CFBGN and USTS-ANFIS in terms of **Accuracy** metric. As seen in the graph above, various techniques are represented in X-axis and accuracy value is represented in Y-axis. Kernel function of ANFIS improves the classification accuracy. It is confirmed from results that discussed GLCM-ANFIS yields relatively good **Accuracy** results of 95.5285%, whereas existing ASAVE, USCBF, CFBGN and USTS-ANFISattains only83.2500% ,89.0200% , 91.8600% and 92.7788% respectively.
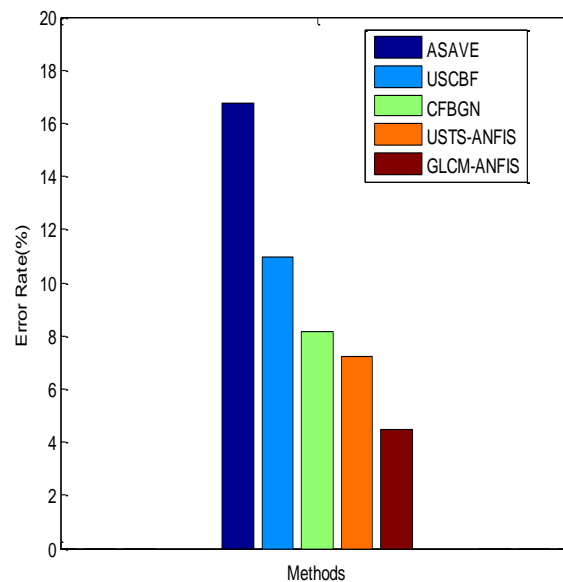
Fig. 12: Error Rate results of different methods

Fig.12 shows Error rate metric analysis comparison carried out between GLCM-ANFIS and the existing ASAVE, USCBF, CFBGN and USTS-ANFIS.

It is confirmed from results that discussed GLCM-ANFIS yields relatively superior Error Rate results of 4.4715% whereas ASAVE, USCBF, CFBGN and USTS-ANFIS attains only 16.7500%, 10.9800%, 8.1400% and 7.2212% respectively.
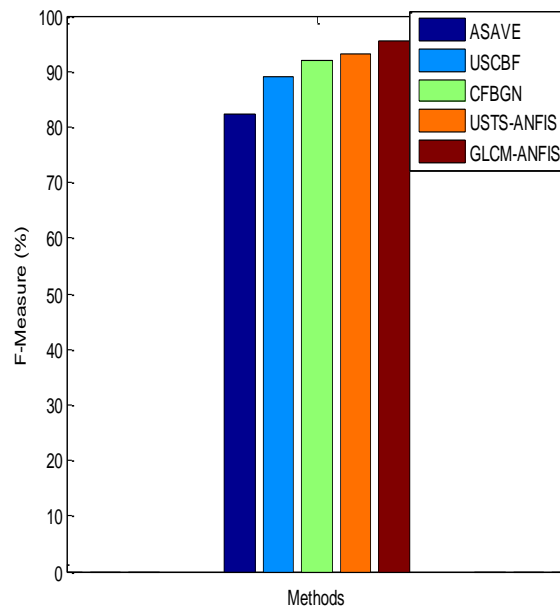
Fig. 13: F-measure results of different techniques

Fig.13. shows performance comparison analysis result between USTS-ANFIS and existing ASAVE, USCBF, CFBGN and USTS-ANFIS with respect to F-measure metric. Gabor filter and image enhancement helps in improving the images performance of region extraction by means of which an improvement in the precision and recall results can be observed.

Then the f-measure results of the discussed system also increases automatically. It is confirmed from results that discussed USTS-ANFIS yields relatively better F-measure values of 95.5338% whereas the existing ASAVE, USCBF, CFBGN and USTS-ANFIS model attains only 82.2900%, 88.9400%, 92.0033 % and 93.0044% respectively.

CONCLUSION AND FUTURE WORK

An innovative enhanced finger vein recognition system is introduced in this research work, where thinning and denoising activities are carried out for the elimination of the unnecessary pixels from the vein pattern. Scattering removal is carried out with the help of dehazing , and in the next step, the Vein   enhancement is carried out through filtering to enhance the vein extraction, then Feature extraction is carried out with the aid of GLCM for the classification performance improvement.

Corner detection is carried out with the help of the Harris corner detection operator and the tracking of the finger vein branches will be performed employing Improved Fuzzy c-means Clustering algorithm. At last, Morphological dilation and dot product operations are carried out on extracted finger vein to improve pixel quality and to get the real or fake finger vein image depending on User-defined threshold employing ANFIS algorithm. But, ANFIS requires massive number of data samples for learning, so that it yields results that are accurate. Hence, the works in future are required to make use of other classifiers for the performance improvement.

REFERENCES

1. Sapkale, M. and Rajbhoj, S.M., 2016, August. A biometric authentication system based on finger vein recognition. In *2016 International Conference on Inventive Computation Technologies (ICICT)* (Vol. 3, pp. 1-4). IEEE.
2. Syazana-Itqan, K., Syafeeza, A.R., Saad, N.M., Hamid, N.A. and Saad, W.H.B.M., 2016. A review of finger-vein biometrics identification approaches. *Indian J. Sci. Technol*, *9*(32)
3. Das, R., Piciucco, E., Maiorana, E. and Campisi, P., 2018. Convolutional neural network for finger-vein-based biometric identification. *IEEE Transactions on Information Forensics and Security*, *14*(2), pp.360-373
4. Liu, Y., Ling, J., Liu, Z., Shen, J. and Gao, C., 2018. Finger vein secure biometric template generation based on deep learning. *Soft Computing*, *22*(7), pp.2257-2265.
5. Basavaraju, R. and Hegde, C., 2017, December. Finger Vein Pattern-based Authentication using Geometrical Properties of Corner Points. In *2017 IEEE International WIE Conference on Electrical and Computer Engineering (WIECON-ECE)* (pp. 145-148). IEEE.

6. Sujani, G. and Reddy, G.S., 2017, June. Finger vein pattern learning models and techniques—A study. In *2017 International Conference on Intelligent Computing and Control Systems (ICICCS)* (pp. 320-323). IEEE.

7. Yang, W., Wang, S., Hu, J., Zheng, G. and Valli, C., 2018. A fingerprint and finger-vein based cancelable multi-biometric system. *Pattern Recognition*, *78*, pp.242-251.

8. Ilankumaran, S. and Deisy, C., 2019. Multi-biometric authentication system using finger vein and iris in cloud computing. *Cluster Computing*, *22*(1), pp.103-117.

9. Hsia, C.H., 2017. New verification strategy for finger-vein recognition system. *IEEE Sensors Journal*, *18*(2), pp.790-797.

10. Carrera, E.V., Izurieta, S. and Carrera, R., 2018, January. A finger-vein biometric system based on textural features. In *International Conference on Information Theoretic Security* (pp. 367-375). Springer, Cham.

11. Das, R., Piciucco, E., Maiorana, E. and Campisi, P., 2018. Convolutional neural network for finger-vein-based biometric identification. *IEEE Transactions on Information Forensics and Security*, *14*(2), pp.360-373.

12. Tagkalakis, F., Vlachakis, D., Megalooikonomou, V. and Skodras, A., 2017, April. A novel approach to finger vein authentication. In *2017 IEEE 14th International Symposium on Biomedical Imaging (ISBI 2017)* (pp. 659-662). IEEE.

13. Yang, W., Hui, C., Chen, Z., Xue, J.H. and Liao, Q., 2019. FV-GAN: finger vein representation using generative adversarial networks. *IEEE Transactions on Information Forensics and Security*, *14*(9), pp.2512-2524.

14. Yang, W., Ji, W., Xue, J.H., Ren, Y. and Liao, Q., 2019. A hybrid finger identification pattern using polarized depth-weighted binary direction coding. *Neurocomputing*, *325*, pp.260-268.

15. Shazeeda, S. and Rosdi, B.A., 2018. Finger vein recognition using mutual sparse representation classification. *IET Biometrics*, *8*(1), pp.49-58.

16. Meng, X., Xi, X., Yang, G. and Yin, Y., 2018. Finger vein recognition based on deformation information. *Science China Information Sciences*, *61*(5), p.052103.

17. Prabu, A.J., 2017. A Biometric Recognition System for Human Identification Using Finger Vein Patterns. *Int. J. Emerg. Trends Eng. Dev.*, *2*(7), pp.62-79.

18. Li, C.Y., Guo, J.C., Cong, R.M., Pang, Y.W. and Wang, B., 2016. Underwater image enhancement by dehazing with minimum information loss and histogram distribution prior. *IEEE Transactions on Image Processing*, *25*(12), pp.5664-5677.

19. Shi, L.F., Chen, B.H., Huang, S.C., Larin, A.O., Seredin, O.S., Kopylov, A.V. and Kuo, S.Y., 2018. Removing haze particles from single image via exponential inference with support vector data description. *IEEE Transactions on Multimedia*, *20*(9), pp.2503-2512.

20. Akintoye, K.A., Shafry, M.R.M. and Abdullah, A.H., 2017. A Novel Approach for Finger Vein Pattern Enhancement using Gabor and Canny Edge Detector. *International Journal of Computer Applications*, *157*(2).

21. Sulaiman, D.M., Abdulazeez, A.M., Haron, H. and Sadiq, S.S., 2019, April. Unsupervised Learning Approach-Based New Optimization K-Means Clustering for Finger Vein Image Localization. In *2019 International Conference on Advanced Science and Engineering (ICOASE)* (pp. 82-87). IEEE.

22. Usha, R. and Perumal, K., 2019. SVM classification of brain images from MRI scans using morphological transformation and GLCM texture features. *International Journal of Computational Systems Engineering*, *5*(1), pp.18-23.

23. Devi, K., Gupta, P., Grover, D. and Dhindsa, A., 2016, September. An effective texture feature extraction approach for iris recognition system. In *2016 2nd International Conference on Advances in Computing, Communication, & Automation (ICACCA)(Fall)* (pp. 1-5). IEEE.

24. Rajawat, A. and Pandey, M.K., 2017, November. Efficient feature extraction using hybrid face recognition method. In *2017 7th International Conference on Communication Systems and Network Technologies (CSNT)* (pp. 158-162). IEEE.

25. ER, A., Varma, S. and Paul, V., 2017. Classification of brain MR images using texture feature extraction. *International Journal of Computer Science and Engineering Communications*, *5*(5), pp.1722-1729.